

## Chapter 3. Superconducting and Quantum-Effect Electronics

### Academic and Research Staff

Professor Terry P. Orlando, Dr. Mauricio Barahona, Dr. Juan Mazo, Dr. Chagarn B. Whan

### Graduate Students

David J. Carter, Janet A. Cutro, Amy E. Duwel, Mark R. Schweizer, Lin Tian, Enrique Trías

### Undergraduate Students

Pieter Heij, Jesper K. Jensen

### Technical and Support Staff

Olga M. Arnold, Angela R. Mickunas

## 3.1 Engineering Josephson Oscillators

### Sponsor

National Science Foundation  
Grant DMR 96-10042

### Project Staff

Enrique Trías, Amy E. Duwel, Professor Terry P. Orlando, Dr. Shinya Watanabe,<sup>1</sup> Dr. Stephen H. Strogatz<sup>2</sup>

As the telecommunications revolution pushes for denser utilization of the spectrum, there is a need to develop inexpensive sources and detectors that operate in the 100 GHz to several THz range. It is precisely in this range that Josephson junctions provide an almost ideal solid state, current controllable source.

Arrays of junctions provide for relatively large power but due to nonlinearities they can exhibit diverse complex spatiotemporal patterns. Experiments, simulations and analysis were performed on a broad range of discrete arrays of Josephson-junction oscillators in order to understand their ability to produce coherent radiation. Networks ranging from single square and triangular plaquettes to one- and two-dimensional arrays are studied. In each array, the junctions are identical and underdamped, and the arrays are driven by dc bias currents. Although few analytical results are known for these systems, we study the technically interesting solutions which can

be represented as traveling waves. It is in this mode that the devices can be used as submillimeter wave sources.

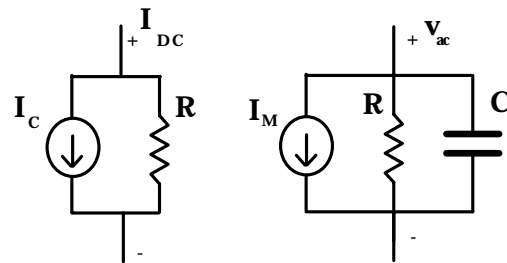


**Figure 1.** Equivalent circuit for a Josephson junction in a voltage state and with a single harmonic. Nonlinearity is captured by  $I_M$  which is a mixing current that describes the interaction between the rotating Josephson phase and its first harmonic.

Using the mathematical technique of harmonic balance it is possible to create an equivalent linear circuit of a Josephson network that is operating in a traveling wave mode. Though the nonlinearity of the system allows for mixing of all the harmonics, in underdamped systems we find that the first harmonic is orders of magnitude stronger than the rest. In general any variable can be decomposed in terms of its dc and ac spectrum. If we further restrict the ac component to a single frequency as suggested by our simulations, then the branch current and voltage across a junction can be written as:

<sup>1</sup> Institute of Mathematics and Applications, University of Minnesota, Duluth, Minnesota.

<sup>2</sup> Cornell University, Ithaca, New York.

$$I = I_{DC} + i_{ac}e^{j\omega t}$$

$$V = V_{DC} + v_{ac}e^{j\omega t}$$

Our equivalent circuit then consists of a dc bias circuit and a mixing circuit that creates the first harmonic. Figure 1 depicts the equivalent circuit. Here

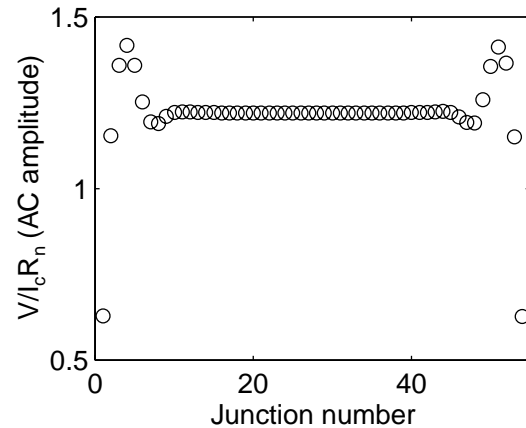
$$I_c = e^{jk}$$

$$I_M = \frac{v_{ac}}{j\omega} \frac{e^{-jk}}{2}$$

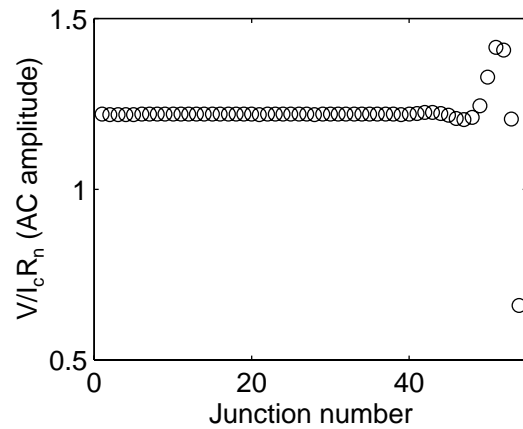
where  $k$  represents the phase difference between the first harmonic and the rotating part of the Josephson oscillation, and the mixing current,  $I_M$ , represents the nonlinear interaction between them. This equivalent circuit makes it possible to use powerful circuit theoretic tools to understand a Josephson network.

A natural application of the circuit model is the study of the effect that the boundaries have on the traveling wave. Figure 2 shows the spatial distribution of first harmonic amplitudes in a parallel Josephson array of 54 junctions. Graph (a) shows the array with open boundaries. In general the shape will depend on the array parameters, but at this value of applied field the spatial part of the solution is symmetric. The reflection of the traveling wave is clearly evident on both the entry and exit sides of the array. Using the above circuit model, it is possible to determine a load impedance that will minimize the reflection. Graph (b) shows the result when the impedance matching load is applied to junction one. The reflection at the left hand boundary is reduced substantially.

We plan to use the linear circuit model to understand how to optimize a Josephson oscillator design so that a minimum of linewidth is obtained while providing a maximum of power and frequency tunability.



(a)



(b)

**Figure 2.** Amplitudes of first harmonics of vertical junctions in a parallel array. Graph (a) is an array with open boundaries while (b) shows the same array with a matching load at junction one.

### 3.2 Triangular Arrays of Josephson Junctions

#### Sponsors

U.S. Air Force - Office of Scientific Research  
Grant F08671-97000989  
Rome Air Force Laboratory

#### Project Staff

Amy E. Duwel, P. Caputo,<sup>3</sup> A. Ustinov,<sup>4</sup> S. Yukon,<sup>5</sup> N.C.H. Lin,<sup>6</sup> Professor Terry P. Orlando

3 KFA, Julich, Germany.

4 Universität Erlangen-Nürnberg, Germany.

5 Rome Air Force Laboratory, Rome, New York.

Triangular arrays of Josephson junctions operating in an applied magnetic field have been proposed as a way of obtaining useful power levels of mm and sub-mm wave radiation generated by the AC Josephson effect. A triangular one-dimensional (1D) array consists of a single row of parallel biased triangular cells which have a Josephson junction in each branch (Figure 3). The bias current is uniformly applied through resistors at each point indicated by arrows in the sketch, and the array voltage response is read across the row. In order to characterize high frequency properties, the horizontal junctions of the array (x-direction) are integrated in an insulating  $\text{SiO}_2$  layer of a superconducting microstripline ending with a finline antenna. The antenna transforms the array impedance into the waveguide impedance through two exponentially tapered Nb fins.

In the presence of a field, two resonances appear on the IV curve, corresponding to  $L_s C$  and  $L_j C$  resonances. These steps are characteristics of single cells, and their voltage does not change with the number of cells in the array. At the  $L_s C$  resonance, triangular arrays produce large-amplitude single-harmonic oscillations in the horizontal junctions. High-frequency measurements of a 12-cell triangular array reveal the presence of radiation emitted from the transverse junctions. Figure 4 shows the radiated power  $P_{\text{rad}}$  at 75 GHz, detected at the  $L_s C$  step. The radiation frequency is proportional to the step voltage. Measurements of longer rows will be taken to test the scaling of power with the number of horizontal junctions.

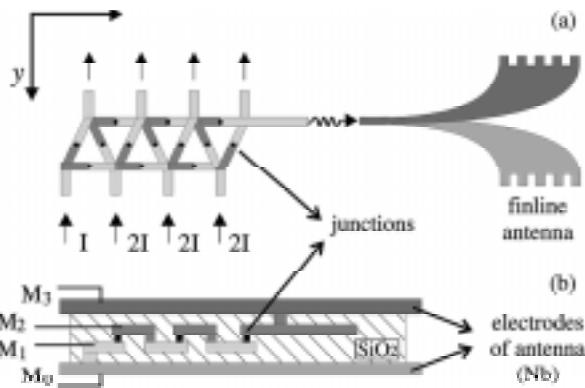


**Figure 3.** Schematic top view of a six-cell triangular array with the finline antenna which couples the array signal to the 80-120 GHz rectangular waveguide (a) and a cross view of the horizontal junctions of the array inserted in the microstripline ending into the antenna (b).

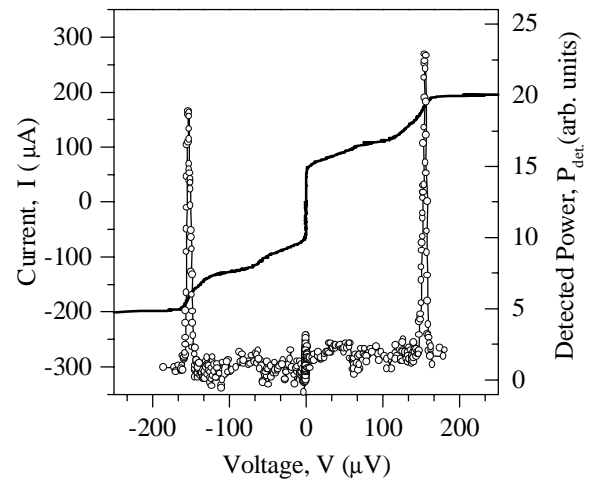


**Figure 4.** Measurement of radiation emission from a 12 cell array. The IV curve is shown together with the detected radiation power at a frequency  $\nu = 75$  GHz. The detector bandwidth is  $\Delta\nu = 0.9$  GHz.

### 3.3 Nonlinear Dynamics Of Discrete Josephson Arrays

#### Sponsors

National Science Foundation  
Grant DMR 96-10042

#### Project Staff

Enrique Trías, Dr. Mauricio Barahona,<sup>7</sup> Professor Terry P. Orlando, Amy E. Duwel, Dr. Herre S.J. van der Zant,<sup>8</sup> Dr. Shinya Watanabe,<sup>9</sup> Dr. Stephen H. Strogatz<sup>10</sup>

Discrete arrays of nonlinear Josephson oscillators can exhibit diverse spatiotemporal patterns. Although such oscillator arrays are difficult to analyze completely, one can often use the symmetries of the system to construct simple patterns composed of spatially repeated “unit cells.” Experiments, simulations, and analysis on a broad class of discrete arrays of Josephson-junction oscillators indicate novel phase-locked states that, due to their special symmetry, reduce the governing equations of the full array to a much smaller set of equations of a unit cell. Networks ranging from single square and triangular plaquettes to one- and two-dimensional arrays have been studied.

6 Rome Air Force Laboratory, Rome, New York.

Figure 5 shows the measured IV curves ( $I$  is the current per vertical junction normalized by  $I_c$ , and  $V$  is the voltage per row) for three different array geometries when fully frustrated. The signature of all these IVs is the appearance of jumps at two resonant voltages,  $V_+$  and  $V_-$ . The upper step, which ends at  $V_+$ , is independent of temperature, suggesting that local geometrical properties determine the voltage. In this state, all the rows of the array act coherently and phase-lock at a voltage that depends on the geometric loop inductance and junction capacitance. The lower voltage  $V_-$ , on the other hand, is temperature-dependent, suggesting a dependence on the Josephson inductance and the geometric loop inductance. By taking advantage of the symmetry of the network, it is possible to describe the solution as a dynamical checkerboard state and mathematically analyze its resonant behavior in a reduced system of governing equations. However, the conditions for the stability and the temporal periodicity of the checkerboard state, and the dynamics associated with other possible states, are challenging problems for future investigation.

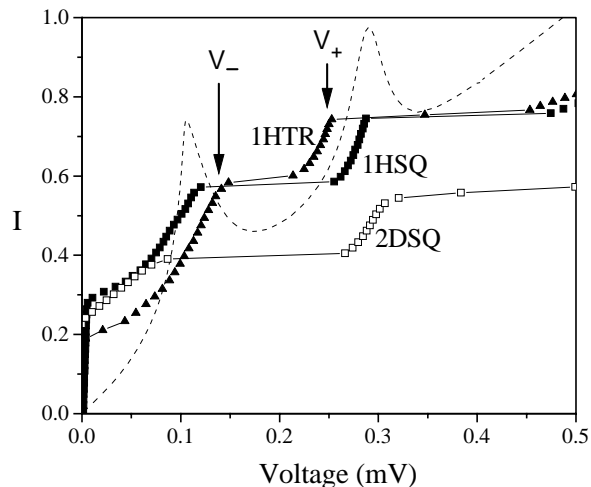


**Figure 5.** Experimental IV curves for three arrays: triangular array (1 X 9 plaquettes) with  $\beta_c = 8$  and  $\lambda = 0.64$ ; square array (1 X 7) with  $\beta_c = 11$  and  $\lambda = 0.76$ ; and a square array (7 X 7) with  $\beta_c = 20$  and  $\lambda = 0.92$ . Dashed line, IV from harmonic balance for the square (1 X 7) array with the same  $\beta_c$  and an effective  $\lambda_{\text{eff}} = 0.61$  which accounts for mutual inductance effects.  $V_+$  and  $V_-$  are indicated.

We have also studied the spatiotemporal dynamics of circular one-dimensional arrays of underdamped Josephson junctions connected in parallel. In these Josephson rings, a traveling wave solution consisting of a single kink can be trapped and studied experimentally without the complications caused by reflections off boundaries. We find that a propagating kink can become phase-locked to linear waves excited in its wake. In the IV curve, resonant steps are observed indicative of this phase-locking. Resonant steps also occur in the IV curves for higher voltages in the return path of the subgap region. These resonant steps have a completely different origin and occur at voltages where the periodic whirling solution undergoes an instability parametrically amplified by the linear modes in the system.

### 3.4 Coupled Rings of Josephson Junctions: Interactions of Topological Kinks

#### Sponsor

National Science Foundation  
Grant DMR 96-10042

#### Project Staff

Amy E. Duwel, Pieter Heij,<sup>11</sup> Enrique Trías, Professor Terry P. Orlando, Dr. Herre S.J. van der Zant,<sup>12</sup> and Dr. Stephen H. Strogatz<sup>13</sup>

We explore a system of two discrete rings of underdamped oscillators, using inductively coupled Josephson junctions as an experimental realization. This Josephson system is a model system for studying spatiotemporal dynamics of coupled oscillators, and more specifically for exploring kink interactions in discrete lattices, a topic that is also important in, e.g., the dynamics of dislocations and ferromagnetic domain walls.

7 Stanford University, Palo Alto, California.

8 Delft University of Technology, The Netherlands.

9 Institute of Mathematics and Applications, University of Minnesota, Duluth, Minnesota.

10 Cornell University, Ithaca, New York.

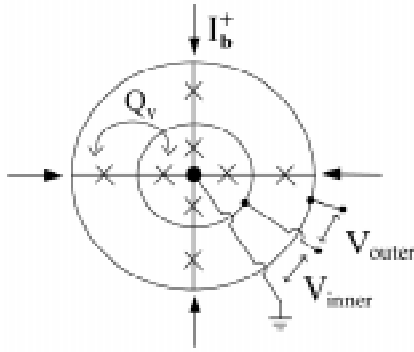


**Figure 6.** Schematic of inductively coupled ring system. A uniform current  $I_b$  is fed into each node, as indicated by arrows and is extracted from the center island. In experiments, we measure the dc voltages  $V_{\text{inner}}$  and  $V_{\text{outer}}$ .  $Q_v$  is the mutual inductance between two adjacent cells of the inner and outer rings.

The layout of a discrete coupled ring system with  $N$  junctions per ring is shown in Figure 6 for  $N=4$ . The Nb-AlO<sub>x</sub>-Nb junctions are  $3 \times 3 \mu\text{m}^2$ , and the radius of the outer ring is  $28 \mu\text{m}$ . When the system is cooled in the presence of a perpendicular magnetic field to below the superconducting transition, the total flux bounded by the continuous superconducting rings becomes trapped in units of  $\phi_0 = h/2e$ . A single unit of quantized flux is called a vortex if the flux is along the applied field and an anti-vortex if it is opposite. A vortex and anti-vortex correspond to a kink and anti-kink. If there are  $m_{v,\text{in}}$  and  $m_{v,\text{out}}$  kinks in the two rings, and  $m_{a,\text{in}}$  and  $m_{a,\text{out}}$  anti-kinks, then the net, conserved phase winding in each ring is  $M_{\text{in}} = m_{v,\text{in}} - m_{a,\text{in}}$  and  $M_{\text{out}} = m_{v,\text{out}} - m_{a,\text{out}}$ .

In Figure 6, we show a simulated IV characteristic for the case of  $M_{\text{in}} = 1$  and  $M_{\text{out}} = 0$ . There are  $N = 51$  junctions in each ring. For a range of bias currents ( $I_b < 0.57 I_c$ ), kink/anti-kink pairs are excited in the outer ring. In the figure, we use an open circle to represent kinks and a cross to represent the anti-kink. The inset shows the relative motions of the kinks and the anti-kink when one pair is excited in the outer ring. As the bias current is applied, the kinks and anti-kink begin to rotate, producing a dc voltage across each ring.

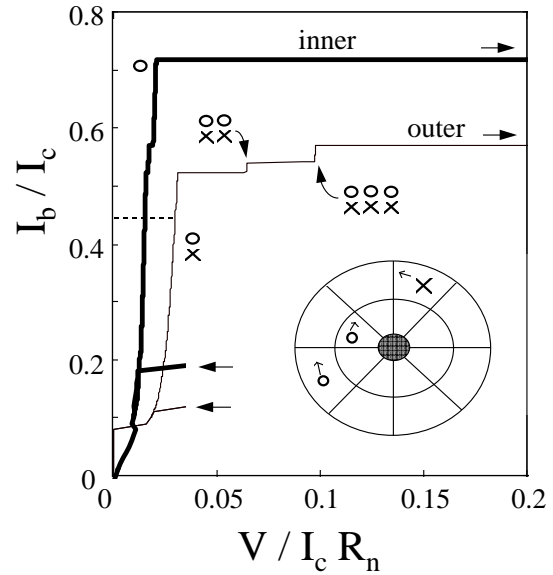


**Figure 7.** Simulated IV characteristic. The nearly constant voltage steps correspond to the motion of the kinks (represented by open circles) and anti-kinks (represented by crosses) at their maximum speeds. The inset shows the relative motion of the kinks and the anti-kink for one excited pair in the outer ring.

In Figure 7, we plot the average dc voltage for each ring versus bias current. As the current is increased, the kinks move faster, and the dc voltage increases. The kinks and anti-kinks phase-lock with linear waves, and, at certain speeds, further increases in the bias current tend to increase the amplitudes of the excited linear waves rather than the speed of a kink. As a result, a step of almost constant voltage appears in the IV. These special speeds are given by the dispersion relation for linear waves in the coupled system, which is split into two branches. We refer to the inner ring step at  $0.0151 I_c R_n$  as an Eck step, since the single trapped kink is near its maximum speed and no additional pairs are excited. When pairs are excited, their contributions simply add up (to lowest order), resulting in voltage steps at much larger voltages. We refer to these as high-voltage (HV) steps, since they are similar to states that can exist on the return path of an isolated ring. A study of the particular dynamics on these steps reveals that the coupling between the rings gives rise to phase-locking between kinks of the same sign in different

11 Delft University of Technology, The Netherlands.

12 Ibid.

13 Cornell University, Ithaca, New York.

rings. The kinks in both rings travel together at the same speeds. The anti-kinks travel in an opposite direction and can even have speeds which are different from the kinks.

In experiments of  $N=4$  and  $N=8$  systems, we discovered another interaction effect. For every distinct combination of  $M_{in} \neq M_{out}$ , we observe a parameter regime where pairs are excited only in the outer ring, another parameter regime where pairs are excited only in the inner ring, and a transition region in temperature from one state to the other. In addition, in several experiments, we observe a very narrow range of temperature where there is a time-dependent competition between the two states. Based on the time scales of the fluctuations, the dynamics are likely to be influenced by weak noise in the input parameters. However, the sudden vulnerability of the system at this particular point also implies the presence of an instability and the possibility of a novel dynamical state. Future experiments will address the role of noise in this two-state competition.

### 3.5 Meissner-like States in Josephson Arrays

#### Sponsor

National Science Foundation  
Grant DMR 96-10042

#### Project Staff

Enrique Trías, Jesper K. Jensen, Professor Terry P. Orlando

One of the most striking features of superconducting materials is their ability to expel an applied flux. This perfect diamagnetism is direct expression of macroscopic quantum mechanical effects and is usually called the Meissner effect. A Meissner state occurs when the induced flux caused by persistent currents in the superconducting material almost perfectly cancels the applied flux.

In order to study this effect in Josephson networks, we designed several ladder arrays with different number of rows. The arrays consist of square loops with junctions on both vertical and horizontal edges. As we increase the applied current from zero, the array is superconducting and therefore has zero output voltage. At some critical current, the array develops a finite voltage, and the zero-voltage state is destroyed. It is in this zero-voltage state that the Meissner state can exist.

To measure the critical current of an array, we first apply a perpendicular magnetic field,  $H_A$ . Once the field is set, the current is swept from zero until the output voltage reaches a threshold value that is typically set to  $1 \mu\text{V}$ . Figure 8 shows representative  $I_{dep}$  versus applied field curves for four different arrays:  $47 \times 47$ ,  $3 \times 47$ ,  $2 \times 47$ , and  $1 \times 15$ . The 47 and 15 refer to the number cells in the direction normal to current injection while the smaller number is the number of rows in the direction of the applied current.

We find generic features for all the measurements regardless of temperature or array topology. First, the shape of the  $I_{dep}$  curves is periodic with the applied field. We normalize the applied field so that  $f = H_A/H_{period}$  and the curves become periodic with  $f = 1$ . Secondly, the curves are almost symmetric about  $f = 0.5$ . The details of the  $I_{dep}$  versus  $f$  curves are sample dependent as shown in Figure 8. For the  $47 \times 47$  ladder, we find that a large narrow peak is observed at  $f=0$ . As  $f$  is increased, the curve quickly decays to an average level of 0.17. There are smaller peaks that are evident at  $f = 1/4$ ,  $f = 1/3$ , and  $f = 1/2$ . The  $3 \times 47$  array has similar features to the fully two-dimensional system. The peak at  $f = 0$  is now broader as marked by the arrow. The decay to the average level is linear but the substructure appears at different  $f$  values. When the array only has two rows, we see curves typical to the  $2 \times 47$  ladder. The  $f = 0$  peak is now very broad, but the decay is still linear. All the other structure has disappeared except for the  $f = 0.5$  peak. Finally, when we measure an array with only one row, the  $f = 0$  peak has expanded so that even the  $f = 0.5$  substructure has disappeared. It is this peak at  $f = 0$  that can be described as a Meissner-like state.

After performing numerical simulations to characterize the Josephson network dynamics, we have developed a model that reproduces the experimental characteristics. We find that even if the geometrical inductances are neglected, the Josephson junctions that circumvent the network can act as parametric inductors that support a circulating current. As the network becomes more two-dimensional it becomes increasingly difficult to support the large circulating current and so the Meissner-like state narrows. The linear decay can be described in terms of Ampère's law. However, it is still not fully understood how the state is destroyed nor what the substructure that is so evident in Figure 8 represents. We will continue to investigate these and other unsolved problems.

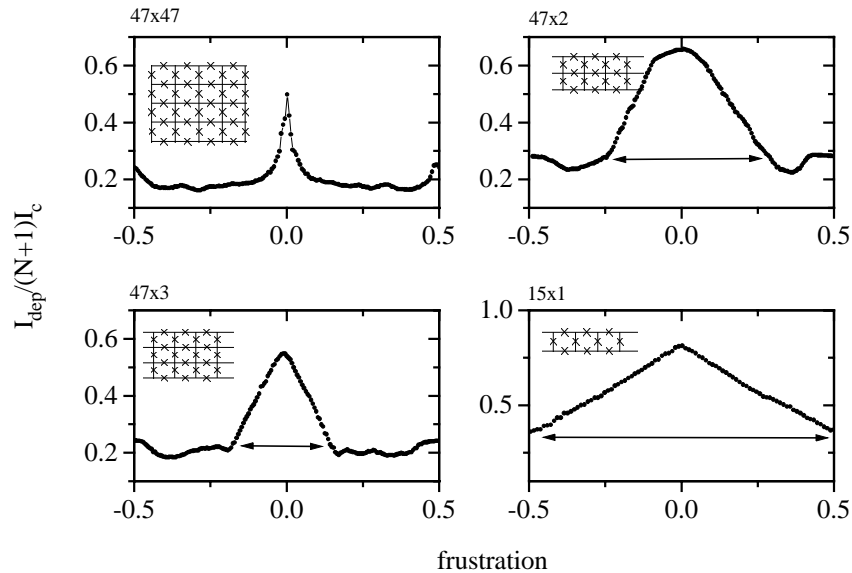


**Figure 8.**  $I_{\text{dep}}$  versus frustration for four different arrays: 47x47, 3x47, 2x47, and 1x15. The 47 and 15 refers to the number cells in the direction normal to current injection while the smaller number is the number of rows in the direction of the applied current. Lines with arrows indicate broadening of  $f=0$  peak as the number of rows of the array decreases.

### 3.6 Self-Field Effects on Flux Flow in Josephson Arrays

#### Sponsor

National Science Foundation  
Grant DMR 96-10042

#### Project Staff

Enrique Trías, Dr. Herre S.J. van der Zant,<sup>14</sup> Professor Terry P. Orlando

Two-dimensional arrays of Josephson junctions provide controllable model systems for the study of vortex transport in thin film superconductors. A crucial parameter that determines the dynamics of these vortices is the characteristic penetration depth of the applied field. It is this length that also governs the effects of self-induced magnetic fields.

Typical current-voltage, IV, characteristics versus applied magnetic field are shown in Figure 9. The applied magnetic field  $B_0$  is measured in units of the frustration  $f = B_0 \rho^2 / \phi_0$ . The depinning current  $I_{\text{dep}}$  indicates the onset of the flux-flow region. There is a

curving transition in the IV from the depinning current to a linear region. The flux-flow resistance  $R_{\text{ff}}$  is defined as the slope of this linear region which is shown by a straight line for each of the IVs. The inset shows that the assigned resistance values are linear in  $f$  up to  $f \approx 0.3$ . For larger values of  $f$  up to  $f = 0.5$ ,  $R_{\text{ff}}$  is no longer linear with  $f$  due to the increased interaction between vortices.

Other measurements and numerical studies of the effects of self-induced magnetic fields on the flux flow resistance have been performed. It was found that the flux-flow resistance becomes larger as the penetration depth of the array decreases. A phenomenological model, which agrees qualitatively with the experiments and simulations, has been developed to explain the self-field effects on flux flow. Due to the smaller spatial extent of supercurrents around a vortex when self-fields are important, both the mass of the vortex and the array viscosity decrease. The decreased mass and viscosity lead to an increase in flux-flow resistance. The effects of spin-wave damping have also been investigated for underdamped arrays.

<sup>14</sup> Delft University of Technology, The Netherlands.

The flux-flow region appears to be richer in its dynamics than the presented model can account for. In particular, treating the effective linear viscosity of the array as the sum of the Bardeen-Stephen damping and spin-wave damping is probably an over-simplification. Though these deviations do not diminish the useful and intuitive results from the phenomenological model, they do point the way for further research on the richness of the dynamics in the flux-flow regime.

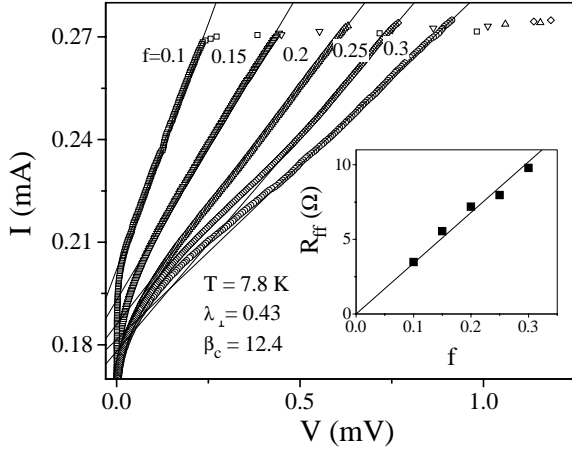


**Figure 9.** Current-voltage characteristics for various magnetic fields from  $f = 0.1$  to  $0.3$ . The data was taken at  $8.6$  K with  $\lambda_{\perp} = 1.04$  and  $\beta_c = 5.1$ . The numbers indicate values of  $f$ . The solid straight lines denote the linear region of flux-flow. The inset shows that the flux-flow resistance  $R_{ff}$  is linear in  $f$ .

### 3.7 Quantum Device Simulations

#### Sponsors

National Science Foundation

Grant DMR 94-02020

U.S. Air Force - Office of Scientific Research

Grant F49-620-92-J-0064

#### Project Staff

Dr. Chagarn B. Whan, Professor Terry P. Orlando

We carried out numerical simulations of single-electron transport through a quantum dot with superconducting leads, based on an experimental system. We introduce a general phenomenological model of transport through a quantum dot. In this model, we assume that the quantum dot is weakly coupled to the two leads by tunnel barriers. When an appropriate bias voltage  $V$  is applied to the leads, an electron

can tunnel across one barrier into the dot and subsequently tunnel out through the second barrier. According to general tunneling theory, the tunneling rate across a barrier from side “a” to side “b”, can be evaluated using Fermi’s Golden Rule,

$$\Gamma_{a \rightarrow b}(\mu_a, \mu_b) = \quad (1)$$

$$\frac{2\pi}{\hbar} \int_{-\infty}^{\infty} |T_{ab}|^2 N_a(E - \mu_a) N_b(E - \mu_b) (f(E - \mu_a) [1 - f(E - \mu_b)]) dE$$

where  $T_{ab}$  is the phenomenological tunneling matrix element, and  $f(x) = 1/[1 + \exp(x/\kappa_B T)]$  is the Fermi function.  $N_a(E)$  and  $N_b(E)$  are the density of states, and  $\mu_a$  and  $\mu_b$  are the chemical potentials, on their corresponding sides. In our system, to compute the tunneling rate from one of the leads to the dot, we take the BCS quasiparticle density of states in the lead and assume that the dot itself has an evenly spaced (with spacing  $\epsilon$ ) discrete level spectrum.

In Figure 10, we show a typical low temperature current-voltage (I-V) characteristic of the system. Here the temperature  $\kappa_B T = 0.02 E_C^*$  ( $E_C^* \equiv E_C + \epsilon$  is the spacing between chemical potential levels, and  $E_C \equiv e^2/C_x$  is the charging energy), the superconducting energy gap  $2\Delta = 0.3 E_C$  and the quantum energy level spacing in the dot  $\epsilon = 0.2 E_C^*$ . When the leads are superconducting (solid curve), the I-V curve consists of a series of sharp peaks spaced  $\epsilon$  apart. This is in contrast with the I-V curve of the same dot with normal metal leads (dashed curve), which has only gentle steps with the same spacing  $\epsilon$ . Figure 10 is in good qualitative agreement with experiment.

In addition to the low temperature transport, our analysis shows that at higher temperatures thermal excitation of quasiparticles in the leads and thermal population of the excited quantum levels within the quantum dot should lead to interesting changes in the I-V curves. We also predict that when RF radiation is coupled to the system, the photon-assisted tunneling phenomenon should manifest itself by producing extra periodic structures in the I-V curves, which might be useful in the millimeter wave detector/mixer applications. Due to the presence of many different characteristic energy scales, the rich dynamical properties of this system demand more exploration.



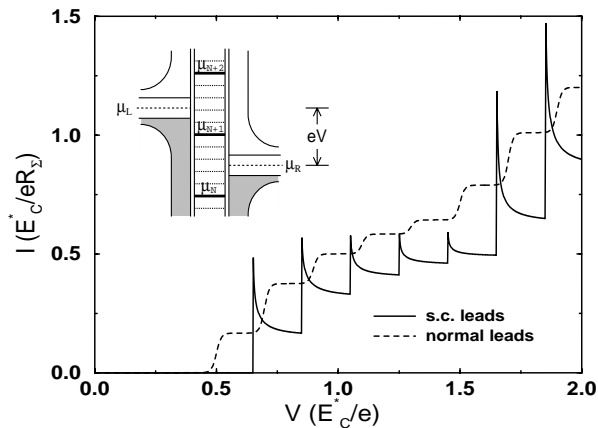


**Figure 10.** Low temperature I-V characteristics of a quantum dot with superconducting leads (solid curve) and normal metal leads (dashed curve). The temperature is  $\kappa_B T = 0.02 E_C^*$ , and the superconducting energy gap in the leads is  $2\Delta = 0.3 E_C^*$ . The quantum level spacing is  $\varepsilon = 0.2 E_C^*$ . The inset is a sketch of the energy spectra in the leads and the dot. Note the quantum dot energy spectrum includes the excitation spectrum (with spacing  $\varepsilon$ ) and addition spectrum (with spacing  $E_C^* = e^2/C + \varepsilon$ ).

### 3.7.1 Publications

- Barahona, M., E. Trías, T.P. Orlando, A.E. Duwel, H.S.J. van der Zant, S. Watanabe, and S.H. Strogatz. "Resonances of Dynamical Checkerboard States in Josephson Arrays with Self-inductance." *Phys. Rev. B* 55: 11989 (1997).
- Barahona, M., S.H. Strogatz, and T.P. Orlando. "Superconducting States and Depinning Transitions of Josephson Ladders." *Phys. Rev. B*. Forthcoming 1998.
- Caputo, P., A.E. Duwel, T.P. Orlando, A.V. Ustinov, N.C.H. Lin, and S.P. Yukon. "Experiments with Triangular Arrays of Josephson Junctions." ISEC, Berlin, 1997.
- Duwel, A.E., T.P. Orlando, S. Watanabe, and H.S.J. van der Zant. "A Novel Phase-Locked State in Discrete Josephson Oscillators." *IEEE Trans. Appl. Superconduct.* 7: 2897 (1997).
- Duwel, A.E., S. Watanabe, E. Trias, T.P. Orlando, and H.S.J. van der Zant. "Discreteness-induced Resonances and AC Voltage Amplitudes in Long One-dimensional Josephson Junction Arrays." *J. Appl. Phys.* 82: 4661-68 (1997).
- Trías, E., M. Barahona, T.P. Orlando, and H.S.J. van der Zant. "Intrinsic Phase-Locked State in Two-dimensional Nb Junction Arrays." *IEEE Trans. Appl. Superconduct.* 7: 3103 (1997).

### Theses

- Cutro, J.A. *Transport Properties and Modification of the Flux Pinning in Single Crystal Bismuth Cuprate Superconductors*. Ph.D. diss., Department of Electrical Engineering and Computer Science, MIT, 1997.
- Jensen, J.K. *Non-linear Dynamics of Josephson Junction Arrays: Expanding the Characteristics of the Depinning Transition from 1D Ladder to 2D Arrays*. B.S. thesis, Department of Electrical Engineering and Computer Science, MIT, 1998.
- Schweizer, M.R. *Fabrication and Measurement of Lateral-surface-superlattice Devices*. M.S. thesis, Department of Electrical Engineering and Computer Science, MIT, 1997.

